Oscillations of the rf surface resistance of zinc

A. A. Galkin, V. A. Mishin, L. T. Tsymbal, and A. N. Cherkasov

Physicotechnical Institute, Academy of Sciences of the Ukrainian SSR, Donetsk
(Submitted 27 September 1980)
Zh. Eksp. Teor. Fiz. **80**, 1981–1996 (May 1981)

An experimental investigation was made of the oscillations of the rf surface resistance of zinc plates in a magnetic field H. The differential characteristics of the Fermi surface were investigated in the $(10\bar{1}0)$ and $(11\bar{2}0)$ planes. Three series of oscillations were due to Doppler-shifted cyclotron resonances of holes in the first Brillouin zone and of electrons at the limiting point and on a skew section through the "lens" in the third zone. It was found that oscillations due to electrons at the limiting point of the lens exhibited the properties of the Gantmakher-Kaner oscillations, in contrast to similar oscillations in cadmium which were of strongly pronounced Doppler nature. A model calculation of the nonlocal conductivity in the $\mathbf{H}\|\mathbf{n}\|[0001]$ case was carried out. It was found that the difference between the experimental results in the case of zinc and cadmium was due to the difference between the Fermi surfaces in the second zone and due to a magnetic breakdown between the second and third zones of zinc.

PACS numbers: 71.25.Hc, 72.15.Gd

1. INTRODUCTION

The Fermi surface of zinc has been investigated by a variety of methods (see, for example, Ref. 1 and the references given there) and it is now known quite thoroughly. We shall report an experimental investigation of the Gantmakher–Kaner (GK) oscillations[2] and of the doppleron oscillations[3] of the surface resistance of zinc in a magnetic field. These effects are a physical consequence of a Doppler-shifted cyclotron resonance which gives rise to weakly damped componets of an rf field in a metal.[2-4]

Oscillations of this kind have been observed in many metals. However, for the purpose of the present investigation, the greatest interest lies in the information available on cadmium whose Fermi surface is similar to that of zinc and which has been practically exhaustively investigated from the point of view relevant to the present study.[3,5-7] Among the previous investigations of zinc one should mention that of Mackey *et al.*[8] representing an experimental study of oscillations of the magnetoresistance due to electrons at the limiting point of a "lens" in the third Brillouin zone, and the results of a study of the rf resistance[9] that have not yet been explained satisfactorily.

The period of the GK oscillations is practically equal to the period of the Sondheimer oscillations under dc conditions[10] given by

$$\Delta H_i = \frac{c\cos\theta}{ed}\left|\frac{\partial S}{\partial p_H}\right|_{p_{Hi}}, \qquad (1)$$

which relates the value of this period to the differential characteristics of the Fermi surface. The doppleron oscillation period may generally depend on the magnetic field, reaching (on increase in the field) the value given by Eq. (1). The following notation is used in Eq. (1): p_H is the electron momentum along the magnetic field $\mathbf{H}$; $S(p_H)$ is the area of the section of the Fermi surface by a plane $p_H = \text{const}$; d is the thickness of the investigated metal plate; θ is the angle between the direction of the magnetic field and the normal to the surface of the plate $\mathbf{n}$; p_{Hi} are the coordinates of the points of discontinuity or extrema of the derivative $\partial S/\partial p_H$ considered as a function of p_H.

We observed three series of oscillations which were interpreted on the basis of the available information about the shape and dimensions of the Fermi surface of zinc. Calculation of the nonlocal conductivity based on the model approximation to the Fermi surface of zinc was made in the process of analysis of the experimental results.

2. DESCRIPTION OF THE EXPERIMENTS

We used apparatus of the NMR spectrometer type with a constant sensitivity in the investigated range of magnetic fields. The derivatives of the surface resistance $\partial \mathrm{Re}Z/\partial H$ and $\partial^2 \mathrm{Re}Z/\partial H^2$ were found by the traditional modulation method. A sample was placed in crossed coils, one of which was a component of an oscillatory circuit of an autodyne oscillator, whereas the other was used to produce circular polarization of the exciting field. Measurements were made in the frequency range 2–6 MHz at temperatures 1.8–4.2°K. A static magnetic field was created by a superconducting solenoid or by an electromagnet, and its values were 43 and 15 kOe, respectively. Rotation of a sample in the magnetic field was measured to within 0.1°. In a plane perpendicular to the plane of rotation the alignment was accurate to within ~0.5°.

Three samples 4 mm in diameter and of thickness d amounting to 0.295, 0.84, and 1.26 ± 0.005 mm were made of a cylindrical single crystal of zinc by cleaving along (0001) planes at liquid nitrogen temperature. A shortcoming of these samples was misalignment of the [0001] axis which amounted to ~0.5° for the overall dimensions of a sample. The experimental results were analyzed allowing for the temperature dependence of the thickness of the sample: $d_{4.2\,\mathrm{K}} \approx 0.985 d_{300\,\mathrm{K}}$ (Ref. 11).

3. ANALYSIS OF THE EXPERIMENTAL RESULTS

The three series of oscillations observed in our experiments were labeled P_1, P_2, and P_3. Extremal values of the quantity $R = |\partial S/\partial p_H|/2\pi\hbar$, calculated us-

 0038-5646/81/051030-08$02.40

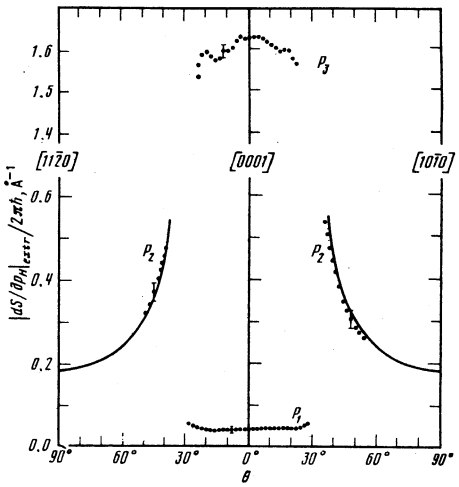

FIG. 1. Experimental values of $|\partial S/\partial p_H|_{extr}/2\pi\hbar$ plotted as a function of the direction of the magnetic field in the (10$\bar{1}$0) and (11$\bar{2}$0) planes. The continuous curves represent the results of a model calculation.

ing Eq. (1) are plotted in Fig. 1. We shall now consider in greater detail each series of oscillations.

1. *Series* P_1. Figure 2 shows the experimental records obtained for the positive and negative polarizations. On the high-field side we can see periodic (in respect of the reciprocal field) quantum oscillations due to the central section of a needle in the third zone. The general nature of these oscillations is demonstrated in Fig. 3. Their characteristic amplitude-field dependence is associated with the existence of the second harmonic of the oscillations and with the filtering effect of differentiation with respect to the magnetic field. The angular dependence of the frequency of these quantum oscillations is in good agreement with the data on the de Haas–van Alphen effect.[12]

In addition to the quantum positively polarized oscillations in fields up to 2.5 kOe, there are also P_1 oscillations with a constant period. The maxima and minima of these oscillations are not shifted when the frequency of the exciting field is altered. The constancy of the period justifies fully the application of Eq. (1) and it is found that the value of R_{extr} for $\mathbf{H}\|[0001]$ is 0.043 ± 0.001 Å^{-1}. The amplitude of the oscillations with the positive polarization is several times greater than the corresponding amplitude in the negative polarization. Hence, we may assume that in the negative polarization the oscillations are of the GK type, whereas in the positive polarization they represent superposition of the GK oscillations and those due to the excitation of hole dopplerons.[1)]

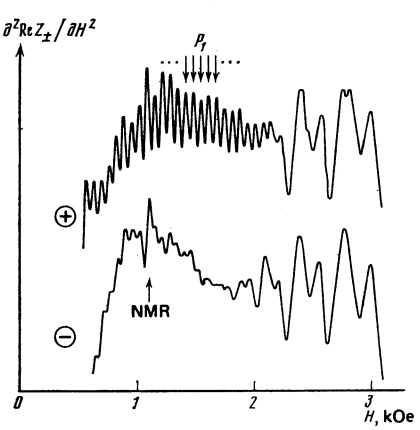

FIG. 2. Records of the second derivative $\partial^2 \mathrm{Re} Z_+/\partial H^2$ obtained in $\mathbf{H}\|\mathbf{n}\|[0001]$, configuration; $T=1.8$°K; $\omega/2\pi=4.6$ MHz; $d=0.295$ mm. The signs of the circular polarization are shown encircled. The arrows identify the P_1-series oscillations and the stray NMR signal.

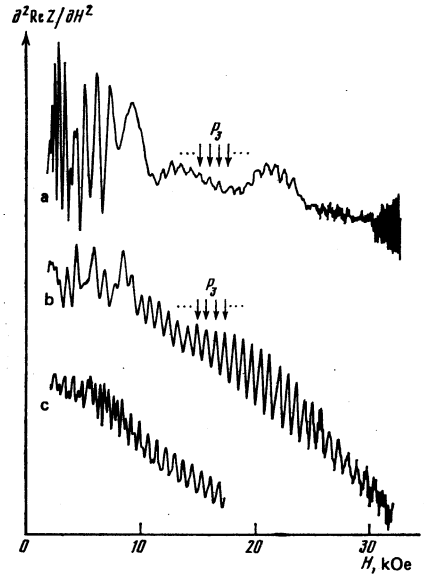

FIG. 3. Records of the second derivative $\partial^2 \mathrm{Re}\, Z/\partial H^2$: *a*) $\theta=0$; *b*) $\theta=10°$, **H** in the (11$\bar{2}$0) plane; *c*) $\theta=16.6°$, **H** in the (10$\bar{1}$0) plane; $T=4.2$ °K, $\omega/2\pi=3.6$ MHz, $d=0.84$ mm. The ordinate scale for curve c is increased compared with the scales for curves a and b. The arrows identify the maxima of the P_3-series oscillations.

The results of Ref. 1 were used to calculate the dependence of R on p_H in the $\mathbf{H}\|[0001]$ geometry for a hole pyramid with its center at the point H (Fig. 4). Figure 5 shows the results of this calculation, estimated to be accurate to within 10%. We can see that the maximum value of R is approximately 0.04 Å^{-1} and

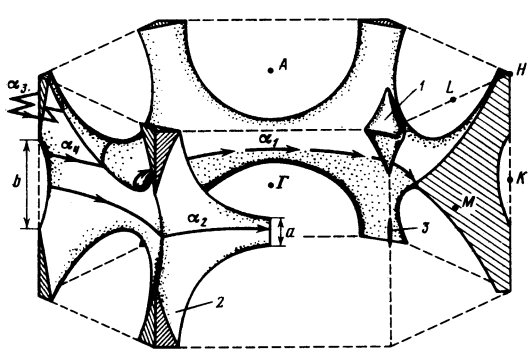

FIG. 4. Fermi surface of zinc: *1*) hole pyramids at the points H in the first zone; *2*) hole monster in the second zone; *3*) electron needles at the point K in the third zone (an electron lens with its center at the point Γ is not shown).

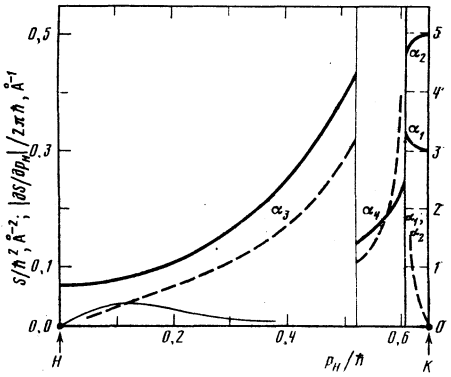

FIG. 5. Graphs representing the derivative $|\partial S/\partial p_H|$ and the areas of the section $S(p_H)$ of the Fermi surface of zinc in the first and second zones in the H‖[0001] configuration. The thick dashed lines represent S and $|\partial S/\partial p_H|$, respectively, for the αi orbits (Fig. 1). The thin curve is the result of a calculation of $|\partial S/\partial p_H|$ for the hole pyramid. The abscissa represents $p_H/\hbar$ (Å^{-1}).

it is close to that found experimentally. A qualitative analysis confirms also the angular dependence of the quantity R_{extr} (Fig. 1). These observations suggest that oscillations in the P_1 series are Doppler-shifted cyclotron resonances of holes in the pyramids in the first Brillouin zone.

2. *Series* P_2. Figure 6 shows examples of the experimental records obtained for the positive and negative polarizations and typical of the range of angles $\theta = 30-60°$. We can see that the curves are superpositions of impedance singularities of the peak type and of sinusoidal oscillations. The amplitude of the latter in the negative polarization is considerably greater than

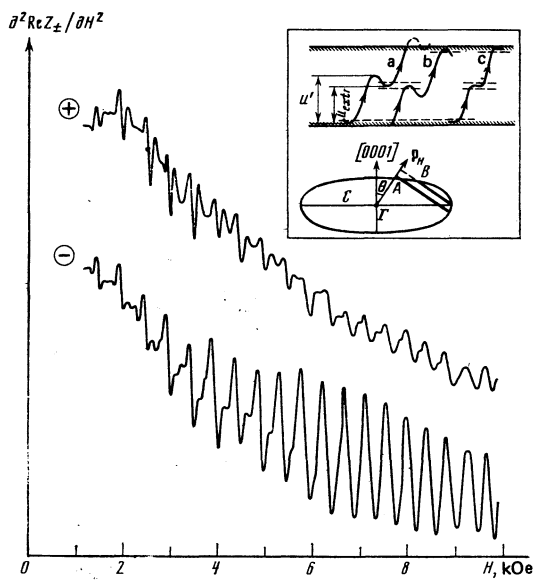

FIG. 6. Records of the second derivative $\partial^2 \mathrm{Re} Z_\pm/\partial H^2$ for $\theta = 39°$ and H in the $(11\bar{2}0)$ plane; $T = 1.8$ °K, $\omega/2\pi = 4.8$ MHz, $d = 0.295$ mm. The signs of the circular polarization are encircled. The inset shows an approximate localization of a skew section of the lens with the maximum value of R (section A). It also gives the nominal projections of the trajectories of the resonance electrons obtained for different angles.

in the positive polarization, indicating clearly the excitation of electron dopplerons (see Footnote 1). The complexity of the oscillation pattern and the narrow range of the frequencies of the exciting field make it impossible to detect the frequency dependence of the threshold field of a doppleron which is approximately 3 kOe.

The sign of the carriers and the characteristic angular dependence of the quantity R_{extr} (Fig. 1) make it possible to identity this series reliably. The inset in Fig. 6 shows an approximate localization of the section of an electron lens with the maximum value of R. In the free-electron model this lens consists of two spherical segments. In this model the cross sections passing through both segments are described by

$$R(p_H,\theta)=\frac{1}{\pi\hbar}\left|\sum_{n=1}^{2}(-1)^n[A\cos\theta+(-1)^n p_H]\times\operatorname{arctg}\frac{[(R_L^2-A^2)\sin^2\theta-p_H^2]^{1/2}}{A\sin^2\theta-(-1)^n p_H\cos\theta}\right|, \quad (2)$$

where p_H is measured from the center of the lens; $A = R_L - p_L$; R_L and p_L are, respectively, the radius and height of the spherical segment. The curves in Fig. 1 represent the results of a calculation of R_{extr} in accordance with Eq. (2) for a lens with the parameters

$$p_L = 0.278\hbar \text{ Å}^{-1}, \quad R_L = 1.63\hbar \text{ Å}^{-1}, \quad (3)$$

the first of which was determined in Ref. 1 and the second was taken as equal to our value of $R_{extr}\hbar$ for the P_3 series in the $\theta = 0$ case (Fig. 1). The experimental results are in good agreement with the calculated dependence of R_{extr} on the angle θ. This means that the oscillations under discussion are associated with a Doppler-shifted cyclotron resonance of electrons belonging to the lens in the third zone. It should be noted that the smaller range of the angles in which the oscillations were observed in the $(10\bar{1}0)$ plane was due to a considerable deterioration of the quality of the relevant sample during measurements caused by the presence of a cleavage plane in zinc.

In addition to the sinusoidal oscillations, Fig. 6 shows impedance singularities of the peak type in both polarizations and these are a consequence of the well known anomalous penetration of the field into a metal assisted by drifting electrons.[14] The peaks appear at $\theta \approx 35°$ reaching the maximum value at $\theta \approx 37°$. The amplitude then decreases and at $\theta \approx 45°$ the peaks are difficult to distinguish against the background of the sinusoidal oscillations which reach their maximum amplitude in this range of angles. Since the repetition period of the peaks is identical with the doppleron oscillation period, it is clear they are both due to the same resonance group of electrons. The inset in Fig. 6 shows an approximate position of the section A near which the resonance electrons are localized. We can see that electrons performing one orbital revolution intersect twice the "effectiveness line" C on which the velocity is parallel to the surface of the sample. The resonance electrons exhibit an extremal shift during a cyclotron period along the normal to the plate (u_{extr}) and, consequently, the rf field peaks may appear at

distances nu_{extr} from the surface. It should be stressed that at distances from the surface amounting to $u' + nu_{extr}$ (inset in Fig. 6, trajectory *a*) there are no field peaks since in this case the displacement u' is not extremal as a function of p_H. In the $u' > u_{extr}$ case, which is typical of the angles $\theta \gtrsim 40°$, the field peaks inside the metal are formed by trajectories of the *a* type that ensure an effective interaction of carriers with the field in the skin layer and are carried to the opposite face along trajectories of the *b* type (multiplication of peaks), whereas the trajectory *a* is cut off by the surface before the field peak reaches the surface. For the angles $\theta \lesssim 40°$ we find from an analysis of the model represented by Eqs. (2) and (3) and from an allowance for the actual shape of the lens that the resonance section *A* along p_H approaches the limiting section *B* intersecting the line *C* at one point. In this case the resonance electrons include those with orbits of the *b* type ($u' \approx u_{extr}$), which give rise directly to a field peak on the opposite side of the plate and this has a large effect on the impedance. The experimentally observed dependence of the peak amplitude on the angle θ is probably due to this circumstance.

3. *Series* P_3. Figure 3 shows oscillations of the surface resistance of zinc obtained for a linearly polarized rf field. Against the background of quantum oscillations associated with different extremal direction of the Fermi surface, there are oscillations of the P_3 series with a constant period throughout the investigated range (Figs. 3a and 3b). The oscillation maxima show practically no shift along the magnetic field scale when the frequency of the exciting field is varied. The similarity of the value of $R_{extr}\hbar$ in a wide range of angles (Fig. 1) to the radius of the free-electron sphere $p_F = 1.6\hbar$ Å^{-1} indicates that oscillations of the P_3 series are due to a Doppler-shifted cyclotron resonance of electrons at the limiting point of the lens in the third zone. The value $R_{extr} = 1.63 \pm 0.02$ Å^{-1} obtained by us for $\mathbf{H} \| [0001]$ is somewhat less than the value 1.68 Å^{-1} obtained earlier.[8]

A characteristic feature of the P_3 series oscillations is an approximate equality of the maximum oscillation amplitudes in the positive and negative polarizations. Consequently, we can assume that in both cases these oscillations are the GK oscillations, whereas the Doppler oscillations either have very small amplitudes or are altogether absent.

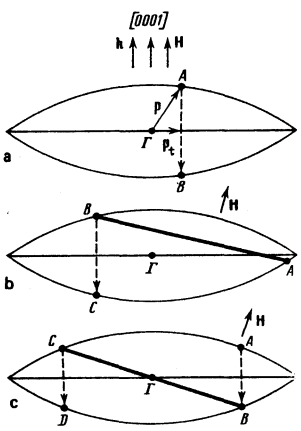

FIG. 7. Specular reflection of electrons at the limiting point of the lens from the surface of a sample for $\mathbf{n} \| [0001]$ and different angles θ.

The amplitude of these ocillations depends in a complex manner on the relative orientation of the magnetic field and the hexagonal axis. When the magnetic field is rotated in the $(11\bar{2}0)$ plane, the oscillation amplitude first rises weakly and then strongly in the range $\theta > 4°$, reaching the maximum value of $J \approx 6$ for $\theta \approx 10.5°$ (Figs. 3a and 3b). Next, the amplitude falls to $J \approx 1.2$ for $\theta \approx 16°$ and then arises to a maximum $J \approx 2.2$ for the second time at $\theta \approx 19°$, dropping then to zero. The oscillation amplitude J is the maximum amplitude of the oscillations at a given angle θ taken as unity for $\theta = 0$. When the magnetic field is inclined along other directions, the oscillation amplitude behaves in a similar complex manner. Within a narrow range there are changes only in the amplitudes of the minima and maxima and in the angles at which they are observed.

The somewhat unexpected feature is the small amplitude of the P_3 oscillations at $\theta = 0$ and its severalfold rise at $\theta \approx 10°$, whereas the amplitude of the Sondheimer oscillations[8] is reported to fall to approximately half the initial values. This shows that an increase in the amplitude in our experiments is not associated with the shape of the Fermi surface lens, i.e., it is not associated with the dependence of the "power" of the resonance group of electrons resulting from its angular dependence. We shall show that this complex amplitude-angular dependence of the P_3 oscillations may be due to specular reflection of electrons from the surface of a sample.

Such specular reflection from the surface of a metal represents scattering accompanied by the conservation of energy and of the tangential component of the quasimomentum p_t, i.e., the initial and final states of an electron lie at the points of intersection of the Fermi surface by the straight line $p_t = \text{const}$ (Ref. 15). In the geometry of Fig. 7a the result of the specular reflection $A \to B$ is only a change in the sign of the H component of the electron velocity. The resonance group of electrons is scattered from one limiting point to another and, as shown in Ref. 16, the amplitude of the GK oscillations is considerably less than in the case of diffuse reflection. Since the samples used in our experiments were prepared by cleaving and had surfaces of fairly high quality, one would expect the specular reflection coefficient to be fairly high. Consequently, the small amplitude of the P_3 oscillations at $\theta = 0$ may be due to specular reflection of electrons from the surface of the sample. We shall now use a qualitative analysis given in Ref. 16 and show that when the magnetic field deviates from the normal to the surface of the sample, the oscillation amplitude should increase although the nature of reflection remains specular. An external wave creates a skin electromagnetic field with a wave vector k_s near the surface of a metal, and resonance electrons interact with this field. The effective field acting on a resonance electron under-

going specular reflection is a sum of the effective field acting on this electron before and after collision with the surface and it is proportional to

$$E_{\text{eff}} \sim \frac{1}{k_1 - k_s} + \frac{1}{-k_2 - k_s} \approx \frac{2k_s + (k_2 - k_1)}{k_1 k_2}, \quad (4)$$

where $k_{2,1} = 2\pi/u_{2,1}$: $u_{2,1}$ is the displacement of an electron during a cyclotron period before and after collision. The right-hand side of Eq. (4) is obtained on the assumption that $|k_s| \ll k_1, k_2$. Clearly, $k_1 \neq k_2$ at $\theta = 0$ (Fig. 7a) and the effective field is very small.[16] When the magnetic field deviates from the normal (Fig. 7b) the electrons in the AB section reflected specularly from the surface at the point B are scattered to the limiting point C. In this case we have $k_1 \neq k_2 (k_2 > k_1)$ and the effective field rises. Consequently, the momentum acquired by an electron in the skin layer is higher than that for $\theta = 0$ and this results in the experimentally observed rise of the amplitude of the P_3 oscillations.

We shall complete our analysis by considering the situation shown in Fig. 7c. After the $A \to B$ specular reflection an electron makes half a revolution along the orbit of the central section BC and at the point C it is scattered for the second time by the same surface. Consequently, the resonance electrons arriving at the surface of a plate consist of two groups. The first comprises those electrons which are localized in the vicinity of the limiting point A, and the second comprises those in the vicinity of the limiting point C (after the $A \to BC$ specular reflection, see Fig. 7c). The signal carried to the surface by the electrons of the second group is shifted in phase by π relative to the signal due to the electrons of the first group and this is the result of revolution along the orbit in the BC section. Since the experimental results give the sum of two oscillating signals which are opposite in phase, the resultant amplitude of the P_3 oscillations will be very small. In the model (3) the situation shown in Fig. 7c appears at $\theta = 19°$, whereas the minimum of the amplitude of the P_3 oscillations is located at $\theta \approx 16.5°$. The discrepancy between these two angles is slight and it is probably due to the fact that there is a small difference between the model (3) and the real Fermi surface.

We shall consider one other feature of the P_3-series oscillations. The fall of the oscillation amplitude near $\theta \approx 16.5°$ is accompanied by the appearance of oscillations with a period approximately half the period of the main oscillations. Figure 7c demonstrates this singularity in the geometry in which it appears particularly clearly. These oscillations are most probably not a harmonic of the main signal but appear as a result of the addition of two signals with opposite phases, as discussed above, when these signals are not purely sinusoidal. However, it should be pointed out that, as a result of double specular reflection $A \to BC \to D$ (Fig. 7c), we can observe the second harmonic of the P_3 oscillations when the path is sufficiently long, because the point D (like the point A) is limiting. But then the harmonic should be observed also for $\theta = 0$ (Fig. 3a), since in this case only one specular reflection is needed. However, no doubling of the P_3 oscillations was observed in this geometry.

4. THEORETICAL ANALYSIS AND COMPARISON WITH THE EXPERIMENTAL RESULTS

We shall now write down the relationships needed in our analysis. It is known that when the magnetic field direction, axial symmetry axis, and the normal to the surface of a sample all coincide, the conductivity tensor can be diagonalized in terms of circularly polarized components of the electric field $E_\pm = E_x \pm iE_y$. The spectrum of electromagnetic modes is governed by the dispersion relationship (for details of this part of the treatment and later stages see, for example, Refs. 3 and 4)

$$k^3c^3 = 4\pi i\omega\sigma_\pm(k), \quad (5)$$

where $\sigma_\pm = \sigma_{xx} \pm i\sigma_{yx}$ is a nonlocal conductivity for a circularly polarized field; ω and k are the frequency and wave vector of an electromagnetic mode. It should be noted that the requirement of axial simplifies the problem greatly and does not restrict its validity as long as we do not discuss the specific phenomena associated with the Fermi surface symmetry. Introducing the dimensionless parameters

$$q = \frac{k}{2\pi/u_L} \text{ and } \xi = \frac{\pi e H^3}{N_e c |\partial S/\partial p_H|_L^2 \omega}, \quad (6)$$

we shall rewrite the dispersion equation (5) in the collisionless limit for $\omega_c \gg \omega$ in the form

$$\mp q^2 \xi = F(q) \quad (\pm \text{ polarization}), \quad (7)$$

where $F(q)$ is a nonlocal factor in the conductivity

$$\sigma_\pm = \pm i \frac{N_e ec}{H} F(q), \quad (8)$$

defined by the relationship

$$F(q) = \sum_j \frac{N_j}{N_e} F_j(q), \quad (9)$$

$$F_j(q) = \int \frac{S(p_H)\,dp_H}{1 - q(\partial S/\partial p_H)/|\partial S/\partial p_H|_L} \left[\int S(p_H)\,dp_H\right]^{-1} \operatorname{sgn} m, \quad (10)$$

$$N_j = \frac{2}{(2\pi\hbar)^3} \int S(p_H)\,dp_H. \quad (11)$$

The following notation is used above; ω_c is the cyclotron frequency; N_e is the total density of electrons; $\operatorname{sgn} m$ is the sign of the cyclotron mass of the carriers; Σ_j is the symbol denoting summation over selected parts of the Fermi surface where the density N_j; $u_L = c|\partial s/\partial p_H|_L/eH$ is the displacement (during one cyclotron period), introduced here for convenience in our analysis, of the electrons at the limiting point of the lens, the integrals are taken over the selected parts of the Fermi surface.

1. *Analysis of the Fermi surface of zinc.* Like cadmium, zinc is a compensated metal, i.e., the volumes of the electron and hole parts of the Fermi surface are equal. The parameters of the hole pyramid in the first Brillouin zone and of the electron lens in the third zone differ slightly (in the quantitative sense) from the parameters of the corresponding surfaces of cadmium. In the absence of reliable experi-

mental data we shall use the results of calculations given in Ref. 17 and assume that there are no electron butterflies and cigars in the third and fourth zones. Consequently, the main difference between the Fermi surfaces of zinc and cadmium (apart from the needles in the third zone whose conductivity contribution can be ignored because of their negligible volume) is the presence of horizontal arms joining together the surface of the hole monster in the second zone (Fig. 4). The connectivity of the monster gives rise in the $\mathbf{H} \| [0001]$ case to electron orbits α_1 on its surface and these contribute to the "electron" component of the conductivity However, since it follows from Ref. 1 that $a<b$ (Fig. 4), there is no geometric decompensation. An increase in the electron density is compensated by the equivalent increase in the density of holes whose appearance is associated with the appearance of hole orbits α_2. The simplicity of the shape of the Fermi surface in the first and third zones makes it possible to calculate the density of the individual groups of carriers in zinc. A calculation made by us on the basis of the results of Ref. 1 gives

$$N_1=(0.029\pm0.0015)\cdot10^{22}\ \text{cm}^{-3},\quad N_3=(0.598\pm0.004)\cdot10^{22}\ \text{cm}^{-3}, \tag{12}$$

where N_j is the density of carriers in the j-th zone.

2. *Nonlocal conductivity.* We shall calculate the nonlocal conductivity in the $\mathbf{H} \| [0001]$ geometry using the models which give qualitatively correct predictions of the dependences of S and of $\partial S/\partial p_H$ on p_H.

We shall approximate the electron lens by a model suggested in Ref. 5:

$$\left.\begin{aligned} \partial S/\partial p_H=-2\pi R_L[1-(1-|p_H|/p_L)^n]\ \operatorname{sgn} p_H,\quad |p_H|\leqslant p_L,\\ S(p_L)=0, \end{aligned}\right\} \tag{13}$$

where $R_L=|\partial S/\partial p_H|_L/2\pi$ is the radius of curvature of the surface of the lens at the limiting point. The model (13) with the parameters of Eq. (3) and $n=4$ describes well all the experimental data on the size effect.[1] It follows from Eq. (10) that

$$F_L(q)=\frac{3}{28q^2}\left[\frac{4q-1}{2}\left(\frac{q}{1+q}\right)^{1/2}\ln\frac{1+[q/(1+q)]^{1/2}}{1-[q/(1+q)]^{1/2}}+(4q+1)\left(\frac{q}{1-q}\right)^{1/2}\operatorname{arctg}\left(\frac{q}{1-q}\right)^{1/2}\right]. \tag{14}$$

The model density of electrons calculated from Eq. (11) is $N_L=0.595\times10^{22}\ \text{cm}^{-3}$, which is practically identical with the calculated value given in Eq. (12).

The hole monster of zinc is strongly anisotropic and the area of its section $S(p_H)$ varies in a complex manner. The presence of saddle points on this monster has the effect that the deriavtive $\partial S/\partial p_H$ has no upper limit. An analysis shows that the dependences of $S(p_H)$ and $\partial S/\partial p_H$ on p_H can be described for all parts of the monster corresponding to the orbits α_1 (Fig. 4) by a fairly simple model of an axially symmetric Fermi surface discussed in Ref. 13:

$$S(p_H)=S''+(S'-S'')[1-(p_H/p_M)^2]^{1/2}. \tag{15}$$

Here, S', S'', and p_H are the parameters of the model. The values of a, b, and ΓA (Fig. 4), which determine the parameters p_M, are assumed—in accordance with

TABLE I.

	α_1	α_2	α_3	α_4
$S'/\hbar^2$, Å^{-2}	3,00	5.00	0,066	0.066/3
$S''/\hbar^2$, Å^{-2}	3.28	4,72	0,8	0,8/3
$p_M/\hbar$, Å^{-1}	0,04		0.61	

Ref. 1—to be

$$a=0.08\hbar\ \text{Å}^{-1},\quad b=0.26\hbar\ \text{Å}^{-1},\quad \Gamma A=0.65\hbar\ \text{Å}^{-1}. \tag{16}$$

The model of almost-free electrons and the results of Refs. 1 and 12 were used to estimate the values of $S(p_H)$ in the ΓKM and AHL planes, in a plane passing through the saddle points, and in a plane separating the orbits α_3 and α_4. Table I gives the values of the parameters S' and S'' slightly different from those used in the estimates and selected in such a way that the density of the holes in the monster is close to the calculated value. For the α_1 and α_2 orbits the value of p_H is measured from the ΓKM plane and we also have $|p_H|\leqslant p_M$. For the orbits α_3 and α_4, the value of p_H is measured from the AHL plane and we also have $|p_H|\leqslant 0.52\hbar$ Å^{-1} for α_3 and $9.52\hbar$ Å$^{-1}\leqslant|p_H|\leqslant p_M$ for α_4. Graphs of the functions $S(p_H)$ and $\partial S/\partial p_H$ are plotted in Fig. 5.

Next, substituting Eq. (16) into Eq. (10), and integrating from $-p_M'$ to p_M' ($p_M'\leqslant p_M$), we obtain

$$F_M(x,\gamma)=\left[\beta\gamma-\frac{\arcsin\gamma}{2}-\frac{\gamma(1-\gamma^2)^{1/2}}{2}+\frac{x^2}{1+x^2}\arcsin\gamma+\frac{\beta x^2}{2(1+x^2)^{1/2}}\ln\frac{1+\gamma(1+x^2)^{1/2}}{1-\gamma(1+x^2)^{1/2}}+\frac{x^3}{2(1+x^2)}\ln\frac{(x(1-\gamma^2)^{1/2}+\gamma+(1+x^2)^{1/2})(1-(1+x^2)^{1/2})}{(x(1-\gamma^2)^{1/2}-\gamma+(1+x^2)^{1/2})(1+(1+x^2)^{1/2})}\right]\left[\left(\beta\gamma-\frac{\arcsin\gamma}{2}-\frac{\gamma(1-\gamma^2)^{1/2}}{2}\right)(1+x^2)\right]^{-1}, \tag{17}$$

where

$$\beta=\frac{S''}{S''-S'},\quad \gamma=\frac{p_M'}{p_M},\quad x=\frac{S''-S'}{p_M}\frac{q}{|\partial S/\partial p_H|_L}. \tag{18}$$

Employing the above formula and substituting the approriate values of S', S'', p_M, and γ, we obtain the functions $F_{M\alpha_i}$ of Eq. (10) for all the selected parts of the Fermi surface monster, which will not be given here because they are too cumbersome. The total density of holes N_M in the monster calculated from Eq. (11) is $0.563\times10^{22}\ \text{cm}^{-3}$. Consequently, the density of the holes in the pyramid is $N_P=0.032\times10^{22}\ \text{cm}^{-3}$ and it is close to the calculated value of Eq. (12).

The dependences of the derivative $\partial S/\partial p_H$ (Fig. 5) and of the area S of the section of the hole pyramid on p_H are of the form typical of a corrugated cylinder Fermi surface, similar to that discussed in Ref. 4. In this model, we have

$$F_P(q)=[1-(q/q_1)^2]^{-1/2},\quad q_1=|\partial S/\partial p_H|_L/|\partial S/\partial p_H|_P, \tag{19}$$

where the value of $|\partial S/\partial p_H|_P$ is assumed to be equal to our experimental value of $0.043\times2\pi\hbar$ [Å^{-1}] (see Sec. 3.1).

Summation of contributions of all the groups of car-

riers in accordance with Eq. (9) gives the function $F(q)$. The results of such a calculation are presented graphically in Fig. 8. We shall consider first the range $q^2<1$. For $\operatorname{Im} F=0$ the solution of the dispersion equation should be the point of intersection of the straight line $q^2\xi$, whose slope is proportional to H^3/ω, and the curve $\operatorname{Re} F$. This graphical solution is shown in Fig. 9. However, the presence of saddle points on the Fermi surface of zinc suppresses the edge of the Doppler-shifted cyclotron absorption. Therefore, we have $\operatorname{Im} F\neq 0$ for any value of q^2 no matter how small. In the range $q^2<1$ the main contribution to $\operatorname{Im} F$ is made by the groups of carriers with the orbits α_1 and α_2. This is due to the fact that the characteristic parameter of the model of Eq. (15) (representing the average derivative $\langle|\partial S/\partial p_H|\rangle=|S''-S'|/p_M$) for the orbits α_1 and α_2 is close to $|\partial S/\partial p_H|_L$, and the areas of these orbits are large. Consequently, the density of carriers participating in the cyclotron asborption of a doppleron wave due to electrons at the limiting point of the lens is considerable.

We can find analytically the dependence of k'' on H ($k=k'+ik''$) by approximating $F(q)$ in the $q^2<1$ case by the function

$$F_1=\eta[(1-q^2)^{-1/2}-1]+iF''q^2. \tag{20}$$

The real part of this function has, like Eq. (14), a square-root singularity and, if $\eta=1.15$, it describes well the curve in Fig. 8. The coefficient F'' can be assumed to be 0.4. Figure 9 shows graphically the solution of the dispersion equation (7) with the function F of Eq. (20). We can see that it is possible to observe the doppleron oscillations in the range $H\gtrsim 20$ kOe and the dispersion of the period will then be slight ($\operatorname{Re} q\approx 1$). However, it is shown in Refs. 4 and 7 that in the range $\operatorname{Re} q\approx 1$ the doppleron oscillation amplitude is proportional to $(1-q)/\omega_c$. Consequently, this amplitude is small and it decreases-in accordance with Eq. (7)-proportionally to H^{-7}.

We shall now consider the doppleron solution of the dispersion equation in the positive polarization case. If $q^2\approx q_1^2$, the imaginary part is $\operatorname{Im} F\sim q^1$ and it is practically constant in the range of interest to us ($\operatorname{Re} F>\operatorname{Im} F$). This allows us to approximate $\operatorname{Im} F$ in this range of values q^2 by the function $-iF''q^2$. The approximation is correct if $\operatorname{Re} q\gg\operatorname{Im} q$ and it allows us to solve the dispersion equation. The function (20) with the parameters $\eta=-N_P/N_L=-0.054$ and $F''=0.16$ describes well the curves plotted in Fig. 8 if we replace q^2 in Eq. (20) with $(q/q_1)^2$. For these parameters and for the frequency under consideration, it follows from Eq. (7) that $k'>k''$ in fields $H>500$ Oe and the dispersion of the period is slight ($\operatorname{Re} q\approx q_1$). Consequently, the experimentally detected P_1-series oscillations do indeed represent a superposition of the doppleron and GK oscillations.

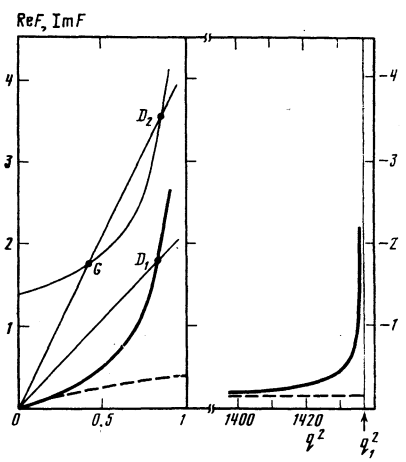

FIG. 8. Graphs showing the real (thick curves) and imaginary (dashed curves) parts of the function $F(q)$. The thin curve is $\operatorname{Re} F(q)$ for $q^2<1$ in the magnetic-breakdown decompensation case. The straight lines are the solutions of Eq. (7) for the negative polarization and $q^2<1$.

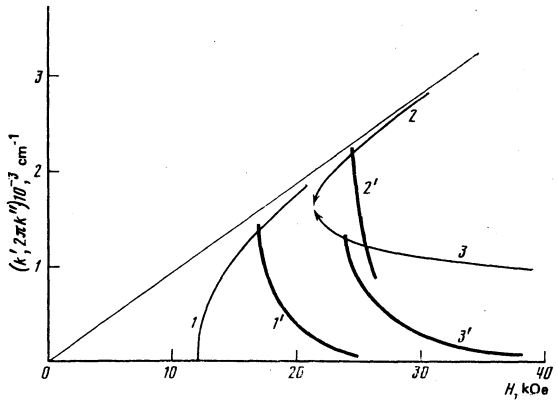

FIG. 9. A straight line represents $q=1$. The thin curves are the results of a graphical solution of Eq. (7) for $\operatorname{Im} F=0$ (see Fig. 8, $q^2<1$): *1*) dependence $k'(H)$ for a doppleron in compensated zinc; *2*), *3*) dependences for a doppleron and a helicon, respectively, in the magnetic-breakdown decompensation case. Curves *1′*, *2′*, and *3′* represent the dependence $2\pi k''(H)$; $\omega/2\pi=3.5$ MHz.

3. *Magnetic breakdown in zinc.* We shall now consider the influence of magnetic breakdown on the nature of the nonlocal conductivity in zinc. The energy gap between the second and third Brillouin zones is small near the point K so that in fields $H\approx 1.3$ kOe (Ref. 18) the hole orbits α_2 begin to disappear and electron orbits corresponding approximately to those in the central section of the free-electron sphere begin to appear.

Decompensation of the electron and hole densities reaches the following value in relatively weak fields ($H\gtrsim 5$ kOe–Ref. 18).

$$\Delta N=N_e-N_h=0.82\cdot 10^{22}\ \text{cm}^{-3}. \tag{21}$$

This result is obtained from Ref. 18, where a report is given of measurements of the thickness of the layer of magnetic-breakdown decompensating orbits, which is $0.079\hbar$ Å^{-1} and is practically identical with the value $a\approx 0.08\hbar$ Å^{-1} of Ref. 1 (Fig. 1).

We shall now calculate the nonlocal conductivity in the case of magnetic-breakdown decompensation. We shall replace the part of the Fermi surface monster corresponding to the α_2 orbits with the surface formed by the magnetic-breakdown orbits and we shall use the same model of Eq. (15) to approximate this surface. Clearly,

the parameters S' and S'' for this surface are, respectively, $2S_0-S'_{\alpha_2}$ and $2S_0-S''_{\alpha_2}$, where S_0 is the area of the section of the Brillouin zone by the (0001) plane ($\Gamma K = 1.575\hbar$ Å^{-1}). It follows from the calculations that the electrons on the magnetic-breakdown decompensating orbits make a practically local contribution to Re F in the $q^2<1$ case. Therefore, the curve Re F calculated earlier is lifted along the ordinate by an amount $\Delta N/N_L = 1.37$ (Fig. 8). The curves Im F passes somewhat higher than before and for $q^2 = 1-0$ we have Im $F = 0.56$.

It is clear from Fig. 8 that in the decompensation case there are (for Im $F = 0$) two solutions of the dispersion equation: the doppleron solution at the point D_2 and the helicon solution at the point G. We shall now calculate damping of these electromagnetic modes approximating $F(q)$ with the function (20) and adding a term which is due to decompensation $\Delta N/N_L$ on the assumption that $F'' = 0.55$. The solution of Eq. (7) is shown graphically in Fig. 9. We can see that, in principle, the doppleron oscillations can be observed in fields $H \gtrsim 25$ kOe. However, in this range of fields the value of Re q is practically equal to unity. Consequently, the doppleron oscillation amplitude should be even less than in the case of compensated zinc discussed above and it should decrease proportionally to H^{-7}. In our experiments the P_3-series oscillations had no threshold magnetic field higher than 10 kOe and they showed no significant dependence of the amplitude on the sign of the circular polarization of the exciting field. Therefore, on the basis of the above analysis we may conclude that these ocillations are of the *GK* type and the doppleron oscillations (if present at all) have a small amplitude and cannot be separated from the other oscillations.

We can see from Fig. 9 that the helicon oscillations can be observed in fields $H \gtrsim 30$ kOe. However, these were not observed in our experiments. Possibly the helicon oscillations had a small amplitude and were indistinguishable against the background of the quantum oscillations whose amplitude rose steeply in the range $H > 30$ kOe (Fig. 3a). Moreover, in this range of fields the oscillation period for a sample 0.84 mm thick was large and amounted to ~5 kOe, which again made it difficult to observe the helicon oscillations. Obviously, one would have to reduce the frequency of the exciting field and increase the thickness of the sample in order to observe the helicon oscillations.

CONCLUSIONS

Our analysis has been concerned mainly with the P_3-series oscillations which are, as shown above, of the *GK* type. The absence of oscillations associated with electromagnetic modes is due to a strong damping of these modes related mainly to the presence of the α_1 and α_2 orbits (Fig. 4). However, when the magnetic field is inclined to the normal, the magnetic-breakdown decompensation disappears first at $\theta \approx 2°$ (Ref. 18) and then the α_1 and α_2 orbits also disappear. Consequently, the contributions of these groups of carriers to Im F vanish. At the same time the contribution due to the magnetic Landau damping to Im F begins to rise to a very complex dependence of Im F on the angle θ but determination of this dependence is outside the scope of the present paper.

[1)]This assumption is valid if a doppleron is excited by carriers localized near a section characterized by a local maximum of R. In the case of a minimum of R the sign of the carriers is opposite to the sign of the polarization, as observed, for example, in the case of copper.[13]

[1]O. L. Steenhaut and R. G. Goodrich, Phys. Rev. B 1, 4511 (1970).
[2]V. F. Gantmakher and É. A. Kaner, Zh. Eksp. Teor. Fiz. **48**, 1572 (1965) [Sov. Phys. JETP **21**, 1053 (1965)].
[3]L. M. Fisher, V. V. Lavrova, V. A. Yudin, O. V. Konstantinov, and V. G. Skobov, Zh. Eksp. Teor. Fiz. **60**, 759 (1971) [Sov. Phys. JETP **33**, 410 (1971)].
[4]D. S. Falk, B. Gerson, and J. F. Carolan, Phys. Rev. B 1, 406 (1970).
[5]O. V. Konstantinov, V. G. Skobov, V. V. Lavrova, L. M. Fisher, and V. A. Yudin, Zh. Eksp. Teor. Fiz. **63**, 224 (1972) [Sov. Phys. JETP **36**, 118 (1973)].
[6]V. P. Naberezhnykh, D. E. Zherebchevskii, L. T. Tsymbal, and T. M. Yeryomenko, Solid State Commun. **11**, 1529 (1972).
[7]V. V. Lavrova, S. V. Medvedev, V. G. Skobov, L. M. Fisher, and V. A. Yudin, Zh. Eksp. Teor. Fiz. **64**, 1839 (1973) [Sov. Phys. JETP **37**, 929 (1973)].
[8]H. J. Mackey, J. R. Sybert, and W. M. Waller, Phys. Rev. B 1, 3979 (1970).
[9]V. P. Naberezhnykh and L. T. Tsymbal, Solid State Commun. **9**, 693 (1971).
[10]E. H. Sondheimer, Phys. Rev. **80**, 401 (1950).
[11]R. W. Meyerhoff and J. F. Smith, J. Appl. Phys. **33**, 219 (1962).
[12]A. S. Joseph and W. L. Gordon, Phys. Rev. **126**, 489 (1962).
[13]V. V. Lavrova, S. V. Medvedev, V. G. Skobov, L. M. Fisher, A. S. Chernov, and V. A. Yudin, Zh. Eksp. Teor. Fiz. **66**, 700 (1974) [Sov. Phys. JETP **39**, 338 (1974)].
[14]V. F. Gantmakher and É. A. Kaner, Zh. Eksp. Teor. Fiz. **45**, 1430 (1963) [Sov. Phys. JETP **18**, 988 (1964)].
[15]A. F. Andreev, Usp. Fiz. Nauk **105**, 113 (1971) [Sov. Phys. Usp. **14**, 609 (1972)].
[16]I. F. Voloshin, S. V. Medvedev, V. G. Skobov, L. M. Fisher, and A. S. Chernov, Zh. Eksp. Teor. Fiz. **71**, 1555 (1976) [Sov. Phys. JETP **44**, 814 (1976)].
[17]R. W. Stark and L. M. Falicov, Phys. Rev. Lett. **19**, 795 (1967).
[18]W. A. Reed and G. F. Brennert, Phys. Rev. **130**, 565 (1963).
[19]É. A. Kaner and V. G. Skobov, Zh. Eksp. Teor. Fiz. **45**, 610 (1963) [Sov. Phys. JETP **18**, 419 (1964)].

Translated by A. Tybulewicz